Ultrasensitive Atomic Spin Measurements with a Nonlinear Interferometer

R. J. Sewell,[1, *] M. Napolitano,[1] N. Behbood,[1] G. Colangelo,[1] F. Martin Ciurana,[1] and M. W. Mitchell[1, 2]

[1] ICFO-Institut de Ciencies Fotoniques, Mediterranean Technology Park, 08860 Castelldefels (Barcelona), Spain
[2] ICREA - Institució Catalana de Recerca i Estudis Avançats, 08015 Barcelona, Spain

(Dated: June 3, 2014)

We study nonlinear interferometry applied to a measurement of atomic spin and demonstrate a sensitivity that cannot be achieved by any linear-optical measurement with the same experimental resources. We use alignment-to-orientation conversion, a nonlinear-optical technique from optical magnetometry, to perform a nondestructive measurement of the spin alignment of a cold ^{87}Rb atomic ensemble. We observe state-of-the-art spin sensitivity in a single-pass measurement, in good agreement with covariance-matrix theory. Taking the degree of measurement-induced spin squeezing as a figure of merit, we find that the nonlinear technique's experimental performance surpasses the theoretical performance of any linear-optical measurement on the same system, including optimization of probe strength and tuning. The results confirm the central prediction of nonlinear metrology, that superior scaling can lead to superior absolute sensitivity.

I. INTRODUCTION

Many sensitive instruments naturally operate in nonlinear regimes. These instruments include optical magnetometers employing spin-exchange relaxation-free [1] and nonlinear [2] magneto-optic rotation and interferometers employing Bose-Einstein condensates [3–6]. State-of-the-art magnetometers [7–12] and interferometers [13–20] are quantum-noise limited and have been enhanced using techniques from quantum metrology [21–24].

A nonlinear interferometer experiences phase shifts ϕ that depend on N, the particle number, e.g. $\phi = \kappa N \mathcal{Y}$ for a Kerr-type nonlinearity $\mathcal{Y}$, where κ is a coupling constant. This number-dependent phase implies a sensitivity $\Delta \mathcal{Y} \geq (\kappa N)^{-1} \Delta \phi$, and if the nonlinear mechanism does not add noise beyond the $\Delta \phi = N^{-1/2}$ shot noise, the sensitivity $\Delta \mathcal{Y} \propto N^{-3/2}$ even without quantum enhancement. Such a nonlinear system was identified in theory by Boixo et al. [25] and implemented with good agreement by Napolitano et al. [8, 26]. In contrast, entanglement-enhanced linear measurement achieves at best the so-called "Heisenberg limit" $\Delta \phi = N^{-1}$. The faster scaling of the nonlinear measurement suggests a decisive technological advantage for sufficiently large N [25, 27–36]. On the other hand, no experiment has yet employed improved scaling to give superior absolute sensitivity, and several theoretical works [37–40] cast doubt upon this possibility for practical and/or fundamental reasons.

Here, we demonstrate that a quantum-noise-limited nonlinear measurement can indeed achieve a sensitivity unreachable by any linear measurement with the same experimental resources. We use nonlinear Faraday rotation by alignment-to-orientation conversion (AOC) [2], a practical magnetometry technique [2], to make a nondestructive measurement of the spin alignment of a sample of ^{87}Rb atoms [11, 41]. AOC measurement employs an optically-nonlinear polarization interferometer, in which the rotation signal is linear in an atomic variable but nonlinear in the number of photons. We have recently used AOC to generate spin squeezing by quantum nondemolition measurement [42], resulting in the first spin-squeezing-enhanced magnetometer [11]. Here we show that this state-of-the-art sensitivity results from the nonlinear nature of the measurement, and could not be achieved with a linear measurement. We demonstrate a scaling $\Delta J_y \propto N_{\mathrm{L}}^{-3/2}$, where N_{L} is the photon number and J_y is an atomic spin-alignment component, in good agreement with theory describing the interaction of collective spin operators and optical Stokes operators. Relative to earlier nonlinear strategies [8], AOC allows increasing N_{L} by an order of magnitude, giving 20 dB more signal and 10 dB less photon shot noise. The resulting spin sensitivity surpasses by 9 dB the best-possible sensitivity of a linear J_y measurement with the same resources (photon number and allowed damage to the state). Theory shows that this advantage holds over all metrologically relevant conditions.

Understanding the limits of such nonlinear measurements has implications for instruments that naturally operate in nonlinear regimes, such as interferometers employing Bose-Einstein condensates [15, 17, 43] and optical magnetometers employing spin-exchange relaxation-free [1] and nonlinear [2] magneto-optic rotation. Similar nondestructive measurements are used in state-of-the-art optical magnetometers [44–46] and to detect the magnetization of spinor condensates [47–49] and lattice gases [19], and are the basis for proposals for preparing [50–53] and detecting [54, 55] exotic quantum phases of ultracold atoms.

---
* robert.sewell@icfo.es

II. NONLINEAR SPIN MEASUREMENTS

We work with an ensemble of $N_A \sim 10^6$ laser-cooled ^{87}Rb atoms held in an optical dipole trap, as illustrated in Fig. 1(a) and described in detail in Ref. [56]. The atoms are prepared in the $f = 1$ hyperfine ground state, and interact dispersively with light pulses of duration τ via an effective Hamiltonian [57]

$$\hat{H}_{\text{eff}} = \kappa_1 \hat{J}_z \tilde{S}_z + \kappa_2 (\hat{J}_x \tilde{S}_x + \hat{J}_y \tilde{S}_y) - \gamma_F \mathbf{B} \cdot \mathbf{F}, \quad (1)$$

where the coupling coefficients $\kappa_{1,2}$ are proportional to the vectorial and tensorial polarizability, respectively, and γ_F is the ground-state gyromagnetic ratio. Here, the operators $\hat{J}_i$ describe the collective atomic spin, and the optical polarization is described by the pulse-integrated Stokes operators $\int dt\, \tilde{S}_i(t) \equiv \hat{S}_i$ (see Appendix A). $\hat{J}_x$ and $\hat{J}_y$ represent the collective spin alignment, i.e., Raman coherences between states with $\Delta m_f = 2$, and $\hat{J}_z$ describes the collective spin orientation along the quantization axis, set by the direction of propagation of the probe pulses. $\hat{S}_x$ and $\hat{S}_y$ describe linear polarizations, while $\hat{S}_z$ is the degree of circular polarization, i.e., the ellipticity.

In regular Faraday rotation, the collective spin orientation $\hat{J}_z$ is detected indirectly by measuring the polarization rotation of an input optical pulse due to the first term in Eq. (1). Typically, the input optical pulse is $\hat{S}_x$-polarized, and the polarization rotation is detected in the $\hat{S}_y$ basis. Detection of the collective spin alignment J_y (or J_x) requires making use of the second term in Eq. (1), and can be achieved with either a linear or a nonlinear measurement strategy, as we now describe (see Figure 1).

In a linear measurement the polarization rotation due to the term $\kappa_2 \hat{S}_y \hat{J}_y$ is directly measured – e.g., an input $\hat{S}_x$-polarized probe (i.e. $\langle \hat{S}_x \rangle = N_L/2$) is rotated toward $\hat{S}_z$ by a small angle $\Phi_{\text{LTE}} = \kappa_2 \hat{J}_y$. We refer to this type of strategy as linear-to-elliptical (LTE) measurement of J_y. It gives quantum-limited sensitivity

$$(\Delta J_y)^2_{\text{LTE}} = \frac{(\Delta \hat{S}_z^{(\text{in})})^2}{\kappa_2^2 S_x^2} = \frac{1}{\kappa_2^2} \frac{1}{N_L}, \quad (2)$$

i.e., with shot-noise scaling. Here and in the following we use the notation $J_y \equiv \langle \hat{J}_y \rangle$ for expectation values. The same sensitivity is achieved with other linear measurement strategies employing different input polarizations. Note that for large detunings, $\kappa_1 \propto \Delta^{-1} \gg \kappa_2 \propto \Delta^{-2}$, so detection of J_y with this method is less sensitive than regular Faraday-rotation detection of $\hat{J}_z$.

AOC measurement of J_y employs $\hat{H}_{\text{eff}}$ twice and gives a signal nonlinear in N_L: The term $\kappa_2 \hat{S}_x \hat{J}_x$ produces a rotation of $\hat{J}_y$ toward $\hat{J}_z$ by an angle $\theta_{\text{AOC}} = \kappa_2 S_x/2$. Simultaneously, the term $\kappa_1 \hat{S}_z \hat{J}_z$ produces a rotation of $\hat{S}_x$ toward $\hat{S}_y$ by an angle $\Phi_{\text{AOC}} = \kappa_1 \hat{J}_z$. The net effect is an optical rotation $\Phi_{\text{AOC}} = \kappa_1 \kappa_2 N_L \hat{J}_y/4$, which is observed by detecting $\hat{S}_y$. The quantum-noise-limited sensitivity
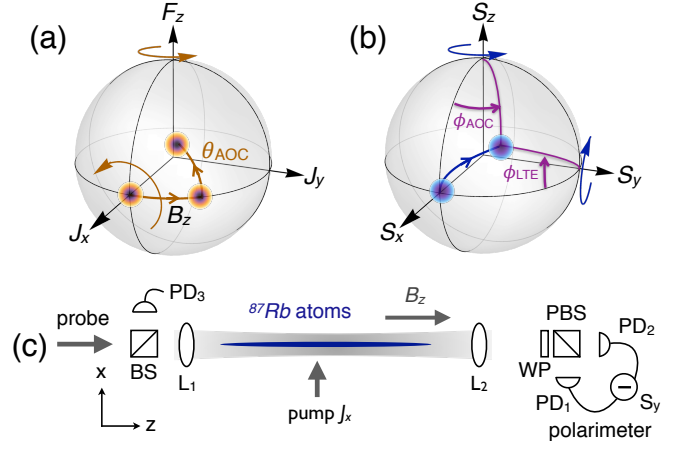

FIG. 1. Alignment-to-orientation conversion measurement of atomic spins. (a) An unknown field B_z rotates an initially $\hat{J}_x$-polarized state in the $\hat{J}_x$-$\hat{J}_y$ plane. The $\hat{J}_y$ component is detected using an $\hat{S}_x$-polarized probe, which produces a rotation of $\hat{J}_y$ toward $\hat{J}_z$ by an angle $\theta_{\text{AOC}} = \kappa_2 \hat{S}_x/2$. (b) Simultaneously, paramagnetic Faraday rotation produces a rotation of $\hat{S}_x$ toward $\hat{S}_y$. The net effect is a rotation $\Phi_{\text{AOC}} = \kappa_1 \kappa_2 N_L \hat{J}_y/4$, which is observed by detecting $\hat{S}_y$. In an alternative strategy, the linear-to-elliptical rotation of $\hat{S}_x$ towards $\hat{S}_z$ by the angle $\Phi_{\text{LTE}} = \kappa_2 \hat{J}_y$ can be observed by detecting $\hat{S}_z$. (c) Experimental geometry. Near-resonant probe pulses pass through a cold cloud of ^{87}Rb atoms and experience a Faraday rotation by an angle proportional to the on-axis collective spin $\hat{J}_z$. Atoms are prepared in a coherent spin state $\hat{J}_x$ via optical pumping. The pulses are initially polarized with maximal Stokes operator $\hat{S}_x$, measured at the input by photodiode (PD$_3$). Rotation toward $\hat{S}_y$ is detected by a balanced polarimeter consisting of a waveplate (WP), polarizing beam splitter (PBS), and photodiodes (PD$_{1,2}$).

of this nonlinear measurement is (see Appendix C)

$$(\Delta J_y)^2_{\text{AOC}} = \left(\frac{4}{\kappa_2 N_L}\right)^2 \left(\frac{1}{\kappa_1^2 N_L} + \frac{N_A}{4}\right) \quad (3)$$

with scaling $\Delta J_y \propto N_L^{-3/2}$ crossing over to $\Delta J_y \propto N_L^{-1}$ at large N_L. Using the Hamiltonian in second order, AOC gives a signal $\propto \kappa_1 \kappa_2 N_L$, versus $\propto \kappa_2$ for LTE, which is an advantage at large detuning, where $\kappa_1 \gg \kappa_2$.

Both strategies employ the same measurement resources, namely, an $\hat{S}_x$-polarized coherent-state probe, so that the quantum uncertainties on the input-polarization angles are $\Delta \hat{S}_y^{(\text{in})}/S_x = \Delta \hat{S}_z^{(\text{in})}/S_x = N_L^{-1/2}$. In addition to the coherent rotations produced by $\hat{H}_{\text{eff}}$, spontaneous scattering of probe photons causes two kinds of "damage" to the spin state: loss of polarization (decoherence) and added spin noise. The tradeoff between information gain and damage is what ultimately limits the sensitivity of the J_y measurement [12, 42, 57]. For equal N_L, the damage is the same for the LTE and AOC measurements, because they have the same initial conditions and differ only in whether $\hat{S}_z$ or $\hat{S}_y$ is detected.

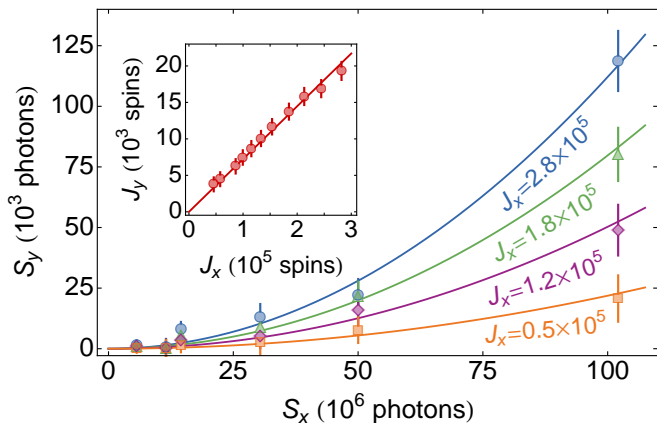From these scaling considerations, the AOC measure-

FIG. 2. Alignment-to-orientation conversion measurement of J_y. In the main frame we plot the signal $S_y = \langle \hat{S}_y^{(\text{out})} \rangle$ of the AOC measurement as a function of S_x for various J_x. We find the measured signal J_y from fit to data using the function $S_y = (\kappa_1 \kappa_2 / 2) J_y S_x^2$ (solid lines). Error bars represent $\pm 1\sigma$ statistical errors. Inset: Measured J_y versus J_x. For small rotation angles $J_y \simeq 2\omega_L B_z t J_x$.

FIG. 3. Log-log plot of the uncertainty ΔJ_y of the AOC measurement versus number of photons N_{L}. Blue diamonds indicate the measured sensitivity. Nonlinear enhanced scaling of the sensitivity is observed over more than an order of magnitude in N_{L}. A fit to the data yields $\Delta J_y \propto N_{\text{L}}^k$ with $k = -1.46 \pm 0.04$. The best observed sensitivity is $\Delta J_y = 1290 \pm 90$ spins with $N_{\text{L}} = 2 \times 10^8$ photons. For reference, we also plot the data (light blue circles) and theory (dotted curve) for the measurement of $\hat{J}_z$ via nonlinear Faraday rotation reported in Napolitano et al. [8] The solid blue curve shows the theoretical prediction given by Eq.(3) with no free parameters, plus the independently measured electronic noise contribution. Dashed green curve: theory curve describing an ideal LTE measurement of J_y without technical or electronic noise contributions. The nonlinear measurement sensitivity surpasses an ideal LTE measurement with $N_{\text{L}} = 3 \times 10^7$ photons. Error bars for standard errors would be smaller than the symbols and are not shown. Inset: Observed metrologically significant spin squeezing ξ_m^2 as a function of photon number. The dashed line is a guide to the eye. Error bars indicate $\pm 1\sigma$ standard errors.

ment should surpass the LTE measurement in sensitivity, $(\Delta J_y)^2_{\text{AOC}} < (\Delta J_y)^2_{\text{LTE}}$ for $N_{\text{L}} \gtrsim 16/(\kappa_1^2 N_{\text{L}}) + 4N_{\text{A}}$, but only if such a large N_{L} does not cause excessive scattering damage to J_y. In atomic ensembles, the achievable information-damage tradeoff is determined by the optical depth (OD) [57], which, in principle, can grow without bound. For high-OD ensembles the nonlinear measurement will, through advantageous scaling, surpass the best-possible linear measurement of the same quantity, under the same conditions. In what follows, we confirm this prediction experimentally, by comparing measured AOC sensitivity to the calculated best-possible sensitivity of the LTE measurement.

III. EXPERIMENTAL DATA AND ANALYSIS

The experimental system, illustrated in Fig. 1(c), is the same as in Ref. [11], with full details given in Ref. [56]. After loading up to 6×10^5 laser-cooled atoms into a single-beam optical dipole trap, we prepare a $\hat{J}_x$-aligned coherent spin state (CSS) via optical pumping, $J_x = \langle \hat{J}_x \rangle = N_{\text{A}}/2$. An (unknown) bias field B_z rotates the state in the $\hat{J}_x$-$\hat{J}_y$ plane at a rate $2\omega_L$, where $\omega_L = -\gamma_F B_z$ is the Larmor frequency, to produce $J_y = \langle \hat{J}_y \rangle = \sin(2\omega_L t) J_x$, which we then detect via AOC measurement. We probe the atoms with a sequence of 2-μs-long-pulses of light sent through the atoms at 5-μs intervals and record $\hat{S}_y^{(\text{out})}$ with a shot-noise-limited balanced polarimeter. The pulses have a detuning $\Delta/2\pi = -600$ MHz, i.e. to the red of the $F = 1 \rightarrow F' = 0$ transition on the D_2 line. To study noise scaling we vary both the number of photons per pulse N_{L}, and the number of atoms N_{A} in the initial
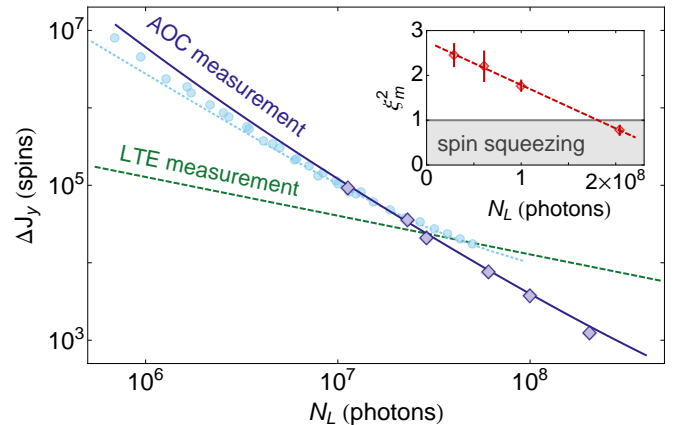
coherent spin state.

In Fig. 2 we plot the observed signal $S_y = \langle \hat{S}_y^{(\text{out})} \rangle$ versus S_x for various values of J_x. The signal is extracted from a differential measurement between the first pulse, a single pulse AOC measurement, and a baseline composite quantum nondemolition measurement constructed from the second and third pulses (see Appendix B). As expected, we observe a signal that increases quadratically with S_x. We extract J_y from a fit to data using the function $S_y = (\kappa_1 \kappa_2 / 2) J_y S_x^2$ (solid lines in Fig. 2), where the coupling constants $\kappa_1 = 1.47 \times 10^{-7}$ rad/spin and $\kappa_2 = 7.54 \times 10^{-9}$ rad/spin are independently measured [11] In the inset we plot the measured J_y versus J_x. For small rotation angles $J_y \simeq 2\omega_L t J_x$, where $t = 7.5\ \mu$s is the time between the centers of the baseline and AOC measurements. A linear fit to the data yields $B_z = 103 \pm 3$ nT.

The measured sensitivity $\Delta J_y = \Delta \hat{S}_y/(\kappa_1 \kappa_2 S_x^2)$ is obtained from the measured readout variation $\Delta \hat{S}_y$ and the slope $\partial S_y/\partial J_y = \kappa_1 \kappa_2 S_x^2$, with the contribution due to the atomic projection noise subtracted (see Appendix C).

As shown in Fig. 3, we observe nonlinear enhanced scaling $\Delta J_y \propto N_L^{-3/2}$ over more than an order of magnitude in N_L. For these data, $J_x = 2.8 \times 10^5$ and $J_y = 1.9 \times 10^4$. The data are well described by the theoretical model of Eq. (3), plus a small offset due to electronic noise, which is independently measured (see Appendix D). We observe a minimum $\Delta J_y = 1230 \pm 90$ spins with $N_L = 2 \times 10^8$ photons.

The AOC measurement sensitivity crosses below the ideal LTE measurement $(\Delta J_y)_{LTE} = (1/\kappa_2)N_L^{-1/2}$ (dashed green line in Fig. 3) with $N_L = 3 \times 10^7$ photons, indicating that, for our experimental parameters, the nonlinear measurement is the superior measurement of $\hat{J}_y$. For comparison, we also compare our measurement of the alignment J_y with the nonlinear Faraday-rotation measurement of J_z reported in Napolitano et al. [8] (light blue circles and dotted line in Fig. 3). We note, in particular, that the advantageous scaling of the current measurement extends to an order-of-magnitude larger N_L than reported in that work.

Nondestructive, projection-noise-limited measurement can be used to prepare a conditional spin-squeezed atomic state [58]. Generation of squeezing is a useful metric for the measurement sensitivity since it takes into account damage done to the atomic state by the optical probe [42, 59]. Here, it is important to note that although the AOC signal is proportional to the atomic spin alignment J_y, quantum noise from the spin orientation $\hat{J}_z$ is mixed into the measurement: Scaled to have units of spins, the Faraday-rotation signal from the AOC measurement is $\hat{\Phi} \equiv (\cos\theta/\kappa_1 S_x)\hat{S}_y^{(out)} = (\cos\theta/\kappa_1 S_x)\hat{S}_y^{(in)} + \hat{K}_\theta^{(in)}$, which describes a nondestructive measurement of the mixed alignment-orientation variable $\hat{K}_\theta^{(in)} \equiv \hat{J}_z^{(in)}\cos\theta + \hat{J}_y^{(in)}\sin\theta$, where $\tan\theta \equiv \kappa_2 S_x/2$ (see Appendix A). $\hat{K}_\theta$ is the variable that should be squeezed to enhance the sensitivity of the AOC measurement. Metrological enhancement is quantified by the spin-squeezing parameter $\xi_m^2 \equiv (\Delta\hat{K}_\theta^{(out)})^2 J_x/2|J_x^{(out)}|^2$ [59] (see Appendix E). With $N_L = 2 \times 10^8$ and $J_x = 2.8 \times 10^5$, we observe a conditional noise 2.3 ± 0.5 dB below the projection noise limit and $\xi_m^2 = 0.7 \pm 0.2$, or 1.5 ± 0.8 dB of metrologically significant spin squeezing (inset of Fig. 3). We note that for our experimental parameters, LTE would not induce spin squeezing.

IV. DISCUSSION

The experiment shows AOC surpassing LTE through improved scaling at the specific detuning of $\Delta/2\pi = -600$ MHz. It is important to ask whether this advantage persists under other measurement conditions. A good metric for the optimum measurement is the number of photons N_L required to achieve a given sensitivity (see Appendix F). In Fig. 4(a) we plot the calculated N_L required to reach projection-noise-limited sensitivity
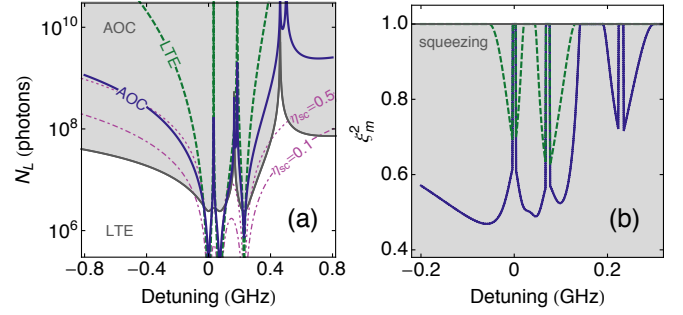

FIG. 4. Theoretical comparison of AOC (solid blue curves) and LTE (dashed green curves) measurement sensitivity. (a) Number of photons N_L needed to achieve projection-noise-limited sensitivity $(\Delta\hat{J}_y)_{AOC}^2 = (\Delta\hat{J}_y)_{LTE}^2 = N_A/4$ as a function of detuning Δ. The gray line indicates $(\Delta\hat{J}_y)_{AOC}^2 = (\Delta\hat{J}_y)_{LTE}^2$, so that the AOC (LTE) strategy is more sensitive in the shaded (white) region. Magenta curves represent damage $\eta_{sc} = 0.1$ (dot-dashed) and 0.5 (dotted) to the atomic state due to spontaneous emission. (b) Estimated metrologically significant spin squeezing ξ_m^2, optimized as a function of N_L, versus probe detuning.

for the two measurement strategies, i.e. $(\Delta J_y)_{AOC}^2 = (\Delta J_y)_{LTE}^2 = N_A/4$ for our experimental parameters. For comparison, we also plot curves showing the damage η_{sc} to the atomic state due to spontaneous emission. We see that the AOC strategy achieves the same sensitivity with fewer probe photons (and thus causes less damage) except very close to the atomic resonances, i.e. except in regions where large scattering rates make the quantum non-demolition measurement impossible anyway. Another important metric is the achievable metrologically significant squeezing, found by optimizing ξ_m^2 over N_L at any given detuning. In Fig. 4(b) we show this optimal ξ_m^2 versus detuning. The global optimum squeezing achieved by the AOC (LTE) strategy is $\xi_m^2 = 0.47$ (0.63) at a detuning of $\Delta/2\pi = -59$ MHz (77 MHz).

In Fig. 5, we plot the achievable $\xi_{m,min}^2$ as a function of N_L versus both detuning Δ and optical depth OD for the AOC [Fig. 5(a)] and LTE [Fig. 5(b)] strategies. We find that AOC is globally optimum, giving more squeezing, and thus better metrological sensitivity, across the entire parameter range. In Fig. 5(c), we plot the fully optimized spin squeezing, i.e., over Δ and N_L, achievable by the AOC and LTE measurement strategies as a function of OD. This comparison again shows an advantage for AOC, including for large OD, and agrees well with experimental results.

We conclude that: (1) for nearly all probe detunings, if N_L is chosen to give projection-noise sensitivity for LTE, then AOC gives better sensitivity at the same detuning and N_L. The exception is probing very near an absorption resonance, which induces a large decoherence in the atomic state. (2) Considering as a figure of merit the achievable spin squeezing, or equivalently, the magneto-metric sensitivity of a Ramsey sequence employing these measurements [11], the global optimum, including choice
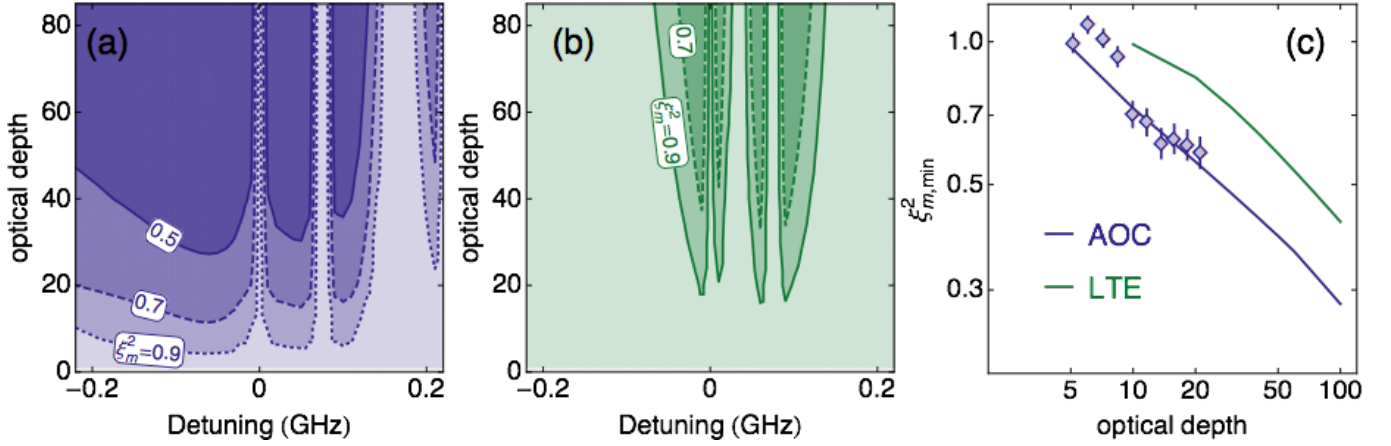
FIG. 5. Theoretical calculation of spin squeezing as a function of optical depth and probe detuning for (a) the AOC strategy and (b) the LTE strategy with our experimental parameters. Contours indicate the minimum achievable metrologically significant squeezing $\xi^2_{m,min}$ with respect to N_L, with values indicated, as a function of detuning Δ and optical depth OD. (c) The blue diamonds represent the observed spin squeezing ξ_m as a function of optical depth for the AOC measurement with $N_L = 2 \times 10^8$ photons. The solid curves show the theoretically predicted minimum achievable squeezing, optimized with respect to both N_L and Δ, for the AOC measurement (solid blue line) and the LTE measurement (solid green line). The scaling of each curve is roughly $\xi^2 \propto OD^{-1/2}$, so the advantage for AOC continues also to large OD.

of measurement, is AOC at a detuning of -59MHz, with $N_L = 5.4 \times 10^6$ photons. In this practical metrological sense, the nonlinear measurement is unambiguously superior. Although the AOC and LTE compared here use coherent states as inputs, the same conclusion is expected when nonclassical probe states are used: For both measurements, the optical rotation sensitivity $\Delta S^{(in)}_{y,z}/S_x$ can be enhanced in the same way by squeezing [7] and other techniques [12].

V. CONCLUSION

We have identified a scenario – nondestructive detection of atomic spin alignment – in which a nonlinear measurement (AOC) outperforms competing linear strategies with the same experimental resources. Our experimental demonstration answers a fundamental question in quantum metrology [37–40], with implications for quantum enhancement of atomic instruments operating in nonlinear regimes [1, 2, 15]. Beyond magnetometry, our techniques may be useful in the measurement of spinor condensates [47–49] and lattice gases [19]. To date, such measurements have been limited to detecting spin orientation (vector magnetization), whereas our technique provides a nondestructive measurement of spin alignment (a component of the spin-one nematic tensor), with direct application, e.g., to the detection of spin-nematic quadrature squeezing in spinor condensates [10]. The technique may make possible proposals for the detection [54, 55] and preparation [51, 52] of exotic quantum phases of ultracold atoms, which require quantum-noise-limited measurement sensitivity.

Appendix A: Atom-light interaction

As described in Refs. [57, 60], the light pulses and atoms interact by the effective Hamiltonian

$$\hat{H}_{eff} = \kappa_1 \hat{J}_z \tilde{S}_z(t) + \kappa_2[\hat{J}_x \tilde{S}_x(t) + \hat{J}_y \tilde{S}_y(t)], \quad (A1)$$

plus higher-order terms describing fast electronic nonlinearities [26]. Here, $\kappa_{1,2}$ are coupling constants that depend on the beam geometry, excited-state linewidth, laser detuning, and the hyperfine structure of the atom, and the light is described by the time-resolved Stokes operator $\tilde{\mathbf{S}}(t)$, defined as $\tilde{S}_i \equiv \frac{1}{2}(\mathcal{E}^{(+)}_+, \mathcal{E}^{(+)}_-)\sigma_i(\mathcal{E}^{(+)}_+, \mathcal{E}^{(+)}_-)^T$, where the σ_i are the Pauli matrices and $\mathcal{E}^{(+)}_\pm(t)$ are the positive-frequency parts of quantized fields for the circular plus or minus polarizations. The pulse-averaged Stokes operators are $\hat{S}_i \equiv \int dt\, \tilde{S}_i(t)$ so that $\hat{S}_i = \frac{1}{2}(a^\dagger_+, a^\dagger_-)\sigma_i(a_+, a_-)^T$, where $a_\pm$ are operators for the temporal mode of the pulse [11]. In all scenarios of interest $\langle \hat{J}_x \rangle \approx N_A/2 \gg \langle \hat{J}_y \rangle, \langle \hat{J}_z \rangle$, and we use input $\hat{S}_x$-polarized light pulses, $S_x = \langle \hat{S}^{(in)}_x \rangle = N_L/2$, and detect the output $\hat{S}^{(out)}_y$ component of the optical polarization.

The atomic spin ensemble is characterized by the operators $\hat{J}_z \equiv \sum_i^{N_A} \hat{f}^{(i)}_z/2$, describing the collective spin orientation, and $\hat{J}_{x,y} \equiv \sum_i^{N_A} \hat{j}^{(i)}_{x,y}$, describing the collective spin alignment, where $\hat{j}_x \equiv (\hat{f}^2_x - \hat{f}^2_y)/2$ and $\hat{j}_y \equiv (\hat{f}_x\hat{f}_y + \hat{f}_y\hat{f}_x)/2$ describe single-atom Raman coherences, i.e., coherences between states with $\Delta m_f = 2$. Here, $\mathbf{f}^{(i)}$ is the total spin of the i th atom. For $f = 1$, these operators obey commutation relations $[\hat{J}_x, \hat{J}_y] = i\hat{J}_z$ and cyclic permutations.

Using Eq. (A1) in the Heisenberg equations of mo-

tion and integrating over the duration of a single light pulse [11], we find the detected outputs to second order in $\hat{S}_x$

$$\hat{S}_z^{(\text{out})} = \hat{S}_z^{(\text{in})} + \kappa_2 \hat{S}_y \hat{J}_x^{(\text{in})} - \kappa_2 \hat{S}_x \hat{J}_y^{(\text{in})} \qquad (\text{A2})$$

$$\hat{S}_y^{(\text{out})} = \hat{S}_y^{(\text{in})} + \kappa_1 \hat{S}_x \hat{J}_z^{(\text{in})} + \frac{\kappa_1 \kappa_2}{2} \hat{S}_x^2 \hat{J}_y^{(\text{in})}$$

$$= \hat{S}_y^{(\text{in})} + \frac{\kappa_1 \hat{S}_x}{\cos\theta} \hat{K}_\theta^{(\text{in})} \qquad (\text{A3})$$

plus small terms. Equation (A3) describes a nondestructive measurement of the mixed alignment-orientation variable $\hat{K}_\theta^{(\text{in})} \equiv \hat{J}_z^{(\text{in})} \cos\theta + \hat{J}_y^{(\text{in})} \sin\theta$, where $\tan\theta \equiv \kappa_2 S_x/2$. $\hat{K}_\theta$ is the variable that should be squeezed to enhance the sensitivity of the AOC measurement.

Appendix B: Measurement signal

We send a train of optical pulses with alternating h- and v-polarization through the atom cloud and record the output Stokes components $\hat{S}_y^{(\text{out,i})}$, $i = 1, 2, \ldots$ and their corresponding inputs $\hat{S}_x^{(\text{in,i})}$. The alternating polarization prevents the rotation angle θ_{AOC} from accumulating, and thus keeps $\hat{S}_y^{(\text{out})}$ within the detector's linear range. We designate the first pulse as the AOC measurement, and use the second and third pulses to construct a baseline quantum nondemolition measurement. We estimate the signal $\langle \hat{J}_y \rangle$ from a differential measurement $\delta \hat{S}_y \equiv \hat{S}_y^{(\text{out,1})} - \hat{S}_y^{(\text{out,b})}$, where $\hat{S}_y^{(\text{out,b})} \equiv (\hat{S}_y^{(\text{out,2})} + \hat{S}_y^{(\text{out,3})})/2$ is is the baseline measurement signal. The AOC measurement signal is then $\langle \hat{J}_y \rangle = 2\langle \delta \hat{S}_y \rangle/(\kappa_1 \kappa_2 \langle \hat{S}_x^{(1)} \rangle^2)$. The composite pulse $\hat{S}_y^{(\text{out,b})}$ constitutes a quantum nondemolition measurement of $\hat{K}_\theta$ [42], and we have previously used such composite pulses to demonstrate spin squeezing of the $\hat{K}_\theta$ variable [11].

Appendix C: Measurement sensitivity

Both AOC and LTE measurements have the same input state, with $S_x \equiv \langle \hat{S}_x^{(\text{in})} \rangle = N_{\text{L}}/2$, $J_x = \langle \hat{J}_x \rangle = N_{\text{A}}/2$, $\langle \hat{J}_z \rangle = 0$, $(\Delta \hat{S}_y^{(\text{in})})^2 = N_{\text{L}}/4$, $(\Delta \hat{J}_z^{(\text{in})})^2 = (\Delta \hat{J}_y^{(\text{in})})^2 = N_{\text{A}}/4$, and uncorrelated $\hat{S}_x, \hat{S}_y, \hat{S}_z, \hat{J}_z,$ and $\hat{J}_y$.

The LTE measurement detects $\hat{S}_z$, with signal $\langle \hat{S}_z^{(\text{out})} \rangle = -\kappa_2 \langle \hat{S}_x \rangle \langle \hat{J}_y \rangle$ and variance $(\Delta \hat{S}_z^{(\text{out})})^2 = (\Delta \hat{S}_z^{(\text{in})})^2 + \kappa_2^2 \langle \hat{J}_x \rangle^2 (\hat{S}_y^{(\text{in})})^2 + \kappa_2^2 \langle \hat{S}_x \rangle^2 (\Delta \hat{J}_y^{(\text{in})})^2$. To infer the $\hat{J}_y$ measurement uncertainty, we note that $\hat{J}_y$ and $\hat{S}_z^{(\text{out})}$ are Gaussian variables [61], so that the simple error-propagation formula coincides with more sophisticated estimation methods using, e.g., Fisher information

[62]. We find:

$$(\Delta \langle \hat{J}_y \rangle)^2 = \frac{(\Delta \hat{S}_z^{(\text{out})})^2}{|\partial \langle \hat{S}_z^{(\text{out})} \rangle/\partial \langle \hat{J}_y \rangle|^2} \qquad (\text{C1})$$

$$= \frac{1}{\kappa_2^2 N_{\text{L}}} + \frac{N_{\text{A}}^2}{4N_{\text{L}}} + \frac{N_{\text{A}}}{4}, \qquad (\text{C2})$$

which shows shot-noise scaling. The first two terms are readout noise and determine the measurement sensitivity. In the experiment $(\kappa_2 N_{\text{A}})^2/4 \sim 10^{-3}$, so the second term is negligible. The last term is due to the variance of $\hat{J}_y$ – i.e., the signal we are trying to estimate – which we subtract to give the expression in Eq. (2). We note that other measurement strategies using the same term in the Hamiltonian are possible, e.g., probing with $\hat{S}_z$-polarized light and reading out the rotation of $\hat{S}_z$ into $\hat{S}_y$, but lead to the same measurement sensitivity.

The AOC measurement detects $\hat{S}_y$, with signal $\langle \hat{S}_y^{(\text{out})} \rangle = (\kappa_1 \kappa_2 \langle \hat{S}_x \rangle^2/2)\langle \hat{J}_y \rangle$ and variance $(\Delta \hat{S}_y^{(\text{out})})^2 = (\Delta \hat{S}_y^{(\text{in})})^2 + (\kappa_1^2 \langle \hat{S}_x \rangle^2)(\Delta \hat{J}_z^{(\text{in})})^2 + (\kappa_1^2 \kappa_2^2 \langle \hat{S}_x \rangle^4/4)(\Delta \hat{J}_y^{(\text{in})})^2$. From this slope and output variance we find the variance referred to the input

$$(\Delta \langle \hat{J}_y \rangle)^2 = \frac{(\Delta \hat{S}_y^{(\text{out})})^2}{|\partial \langle \hat{S}_y^{(\text{out})} \rangle/\partial \langle \hat{J}_y \rangle|^2} \qquad (\text{C3})$$

$$= \frac{16}{\kappa_1^2 \kappa_2^2 N_{\text{L}}^3} + \frac{4N_{\text{A}}}{\kappa_2^2 N_{\text{L}}^2} + \frac{N_{\text{A}}}{4}, \qquad (\text{C4})$$

where again the last term is the signal variance, which we subtract to give the expression in Eq. (3).

In contrast, previous work [8] used short, intense pulses to access a nonlinear term in the effective Hamiltonian $\kappa_{\text{NL}} S_0 \hat{S}_z \hat{J}_z$. The coupling κ_{NL} is proportional to the Kerr nonlinear polarizability, and $S_0 \equiv N_{\text{L}}/2$ (so that $S_0 = \hat{S}_x$ for the input polarization used). Calculating the variance referred to the input as above, we find sensitivity $\Delta J_z = \Delta \hat{S}_z^{(\text{in})}/(\kappa_{\text{NL}} S_x^2)$ and $\Delta J_z \propto N_{\text{L}}^{-3/2}$ scaling.

Appendix D: Electronic & technical noise

The measured electronic noise of the detector referred to the interferometer input is $\text{EN} = 9.2 \times 10^5$ photons, and contributes a term $\text{EN} \times 64/(\kappa_1^2 \kappa_2^2 N_{\text{L}}^4)$ to Eq.(3), which is included in the blue curve plotted in Fig. 3. Technical noise contributions from both the atomic and light variables are negligible in this experiment. Baseline subtraction is used to remove low-frequency noise.

Appendix E: Conditional noise reduction & spin squeezing

Measurement-induced noise reduction is quantified by the conditional variance $\text{var}(\hat{K}_\theta | \Phi_1) = \text{var}(\Phi_b - \chi \Phi_1) - \text{var}(\Phi_{\text{RO}})$, $\hat{\Phi} \equiv (\cos\theta/\kappa_1 S_x)\hat{S}_y^{(\text{out})} = (\cos\theta/\kappa_1 S_x)\hat{S}_y^{(\text{in})} +$

$\hat{K}_\theta$, and $\chi \equiv \mathrm{cov}(\Phi_1, \Phi_b)/\mathrm{var}(\Phi_1) > 0$. Here, $\Phi_1 \equiv (\cos\theta/\kappa_1 S_x^{(1)}) \times \hat{S}_y^{(\mathrm{out},1)}$ and $\Phi_b \equiv (\cos\theta/\kappa_1 (S_x^{(2)} + S_x^{(3)})) \times (\hat{S}_y^{(\mathrm{out},2)} + \hat{S}_y^{(\mathrm{out},3)})$. Spin squeezing is quantified by the Wineland criterion [59], which accounts for both the noise and the coherence of the postmeasurement state: if $\xi_m^2 \equiv 2(\Delta\hat{K}_\theta)^2 J_x/(J_x^{(\mathrm{out})})^2$, where $J_x^{(\mathrm{out})} = (1 - \eta_{\mathrm{sc}})(1 - \eta_{\mathrm{dep}})J_x$ is the mean alignment of the state after the measurement, then $\xi_m^2 < 1$ indicates a metrological advantage. For this experiment, the independently measured depolarization due to probe scattering and field inhomogeneities give $\eta_{\mathrm{sc}} = 0.093$ and $\eta_{\mathrm{dep}} = 0.034$, respectively [11]. The subtracted noise contribution with $N_{\mathrm{L}} = 2 \times 10^8$ photons is $\mathrm{var}(\Phi_{\mathrm{RO}}) = 1.3 \times 10^5$ spins^2.

Appendix F: Dependence on detuning and optical depth

The detuning dependence of the coupling constants κ_1 and κ_2 of Eq.(1) is given by

$$\kappa_1 = \frac{\sigma_0}{A}\frac{\Gamma}{16}\left[-4\delta_0(\Delta) - 5\delta_1(\Delta) + 5\delta_2(\Delta)\right] \quad (\mathrm{F1})$$

$$\kappa_2 = \frac{\sigma_0}{A}\frac{\Gamma}{16}\left[4\delta_0(\Delta) - 5\delta_1(\Delta) + \delta_2(\Delta)\right] \quad (\mathrm{F2})$$

where $\delta_i(\Delta) \equiv 1/\sqrt{\Gamma^2 + (\Delta - \Delta_i)^2}$, Δ_i is the detuning from resonance with the $F = 1 \rightarrow F' = i$ transition on the $^{87}\mathrm{Rb}$ D_2 line, $\Gamma/2\pi = 6.1$ MHz is the natural linewidth of the transition, Δ is measured from the $F = 1 \rightarrow F' = 0$ transition, $\sigma_0 \equiv \lambda^2/\pi$ and $A = 4.1 \times 10^{-9}$ m^2 is the effective atom-light interaction area. Note that for large detuning, i.e., $\Delta \gg \Gamma$, $\kappa_1 \propto 1/\Delta$ and $\kappa_2 \propto 1/\Delta^2$.

At any detuning, the measurement sensitivity can be improved by increasing the number of photons N_{L} used in the measurement. Note, however, that increasing N_{L} also increases the damage $\eta_{\mathrm{sc}} = k(\Delta)\eta_\gamma(\Delta)N_{\mathrm{L}}$ done to the atomic state we are trying to measure due to probe scattering, where $\eta_\gamma(\Delta)$ is the probability of scattering a single photon:

$$\eta_\gamma = \frac{\sigma_0}{A}\frac{\Gamma^2}{64}\left[4\delta_0(\Delta)^2 + 5\delta_1(\Delta)^2 + 7\delta_2(\Delta)^2\right] \quad (\mathrm{F3})$$

which also scales as $\eta_\gamma \propto 1/\Delta^2$ for large detuning. $k(\Delta)$ is a correction factor that accounts for the fact that a fraction of the scattering events leaves the state unchanged. A good metric to compare measurement strategies is the number of photons N_{L} required to achieve a given sensitivity. Minimizing this metric will minimize damage to the atomic state independently of the correction factor $k(\Delta)$. For our calculations, we set $k(\Delta) = 0.4$, which predicts our measurements at large detuning

An estimate for the quantum-noise reduction that can be achieved in a single-pass measurement, valid for $\eta_{\mathrm{sc}} \ll 1$, is given by

$$\xi^2 = \frac{1}{1+\zeta} + 2\eta_{\mathrm{sc}} \quad (\mathrm{F4})$$

where ζ is the signal-to-noise ratio of the measurement, i.e., the ratio of atomic quantum noise to light shot noise in the measured variance $(\Delta\hat{S}_y^{(\mathrm{out})})^2$. For the two strategies considered here,

$$\zeta_{\mathrm{AOC}} = \frac{\kappa_1^2 N_{\mathrm{L}} N_{\mathrm{A}}}{4}\left(1 + \frac{\kappa_2^2 N_{\mathrm{L}}^2}{16}\right) \quad (\mathrm{F5})$$

and

$$\zeta_{\mathrm{LTE}} = \frac{\kappa_1^2 N_{\mathrm{L}} N_{\mathrm{A}}}{4}. \quad (\mathrm{F6})$$

Metrologically significant squeezing is then given by

$$\xi_m^2 = \xi^2/(1 - \eta_{\mathrm{sc}})^2. \quad (\mathrm{F7})$$

[1] J. C. Allred, R. N. Lyman, T. W. Kornack, and M. V. Romalis, *High-sensitivity atomic magnetometer unaffected by spin-exchange relaxation,* Phys. Rev. Lett. **89**, 130801 (2002).

[2] D. Budker, D. F. Kimball, S. M. Rochester, and V. V. Yashchuk, *Nonlinear magneto-optical rotation via alignment-to-orientation conversion,* Phys. Rev. Lett.

85, 2088-2091 (2000).

[3] T. Schumm, S. Hofferberth, L. M. Andersson, S. Wildermuth, S. Groth, I. Bar-Joseph, J. Schmiedmayer, and P. Krüger, *Matter-wave interferometry in a double well on an atom chip,* Nat. Phys. **1**, 57-62 (2005).

[4] G.-B. Jo, J.-H. Choi, C. A. Christensen, Y.-R. Lee, T. A. Pasquini, W. Ketterle, and D. E. Pritchard, *Matter-wave*

interferometry with phase fluctuating bose-einstein condensates, Phys. Rev. Lett. **99**, 240406 (2007).

[5] G.-B. Jo, J.-H. Choi, C. A. Christensen, T. A. Pasquini, Y.-R. Lee, W. Ketterle, and D. E. Pritchard, *Phase-sensitive recombination of two bose-einstein condensates on an atom chip,* Phys. Rev. Lett. **98**, 180401 (2007).

[6] Florian Baumgärtner, R. J. Sewell, S. Eriksson, I. Llorente-Garcia, Jos Dingjan, J. P. Cotter, and E. A. Hinds, *Measuring Energy Differences by BEC Interferometry on a Chip,* Phys. Rev. Lett. **105**, 243003 (2010).

[7] Florian Wolfgramm, Alessandro Cerè, Federica A. Beduini, Ana Predojević, Marco Koschorreck, and Morgan W. Mitchell, *Squeezed-light optical magnetometry,* Phys. Rev. Lett. **105**, 053601 (2010).

[8] M. Napolitano, M. Koschorreck, B. Dubost, N. Behbood, R. J. Sewell, and M. W. Mitchell, *Interaction-based quantum metrology showing scaling beyond the heisenberg limit,* Nature **471**, 486-489 (2011).

[9] Travis Horrom, Robinjeet Singh, Jonathan P. Dowling, and Eugeniy E. Mikhailov, *Quantum-enhanced magnetometer with low-frequency squeezing,* Phys. Rev. A **86**, 023803 (2012).

[10] C. D. Hamley, C. S. Gerving, T. M. Hoang, E. M. Bookjans, and M. S. Chapman, *Spin-nematic squeezed vacuum in a quantum gas,* Nat. Phys. **8**, 305-308 (2012).

[11] R. J. Sewell, M. Koschorreck, M. Napolitano, B. Dubost, N. Behbood, and M. W. Mitchell, *Magnetic sensitivity beyond the projection noise limit by spin squeezing,* Phys. Rev. Lett. **109**, 253605 (2012).

[12] Florian Wolfgramm, Chiara Vitelli, Federica A. Beduini, Nicolas Godbout, and Morgan W. Mitchell, *Entanglement-enhanced probing of a delicate material system,* Nat. Photon. **7**, 28-32 (2013).

[13] J. Esteve, C. Gross, A. Weller, S. Giovanazzi, and M. K. Oberthaler, *Squeezing and entanglement in a bose-einstein condensate,* Nature **455**, 1216-1219 (2008).

[14] Max F. Riedel, Pascal Böhl, Yun Li, Theodor W. Hänsch, Alice Sinatra, and Philipp Treutlein, *Atom-chip-based generation of entanglement for quantum metrology,* Nature **464**, 1170-1173 (2010).

[15] C. Gross, T. Zibold, E. Nicklas, J. Estève, and M. K. Oberthaler, *Nonlinear atom interferometer surpasses classical precision limit,* Nature **464**, 1165-1169 (2010).

[16] C. Gross, H. Strobel, E. Nicklas, T. Zibold, N. Bar-Gill, G. Kurizki, and M. K. Oberthaler, *Atomic homodyne detection of continuous-variable entangled twin-atom states,* Nature **480**, 219 (2011).

[17] B. Luecke, M. Scherer, J. Kruse, L. Pezze, F. Deuretzbacher, P. Hyllus, O. Topic, J. Peise, W. Ertmer, J. Arlt, L. Santos, A. Smerzi, and C. Klempt, *Twin matter waves for interferometry beyond the classical limit,* Science **334**, 773-776 (2011).

[18] Robert Bücker, Julian Grond, Stephanie Manz, Tarik Berrada, Thomas Betz, Christian Koller, Ulrich Hohenester, Thorsten Schumm, Aurélien Perrin, and Jörg Schmiedmayer, *Twin-atom beams,* Nat. Phys. **7**, 608-611 (2011).

[19] Nathan Brahms, Thomas P Purdy, Daniel W C Brooks, Thierry Botter, and Dan M Stamper-Kurn, *Cavity-aided magnetic resonance microscopy of atomic transport in optical lattices,* Nat. Phys. **7**, 604-607 (2011).

[20] T. Berrada, S. van Frank, R. Bücker, T. Schumm, J. F. Schaff, and J. Schmiedmayer, *Integrated Mach-Zehnder interferometer for Bose-Einstein condensates,* Nat. Comm. **4**, 2077 (2013).

[21] Carlton M. Caves, *Quantum-mechanical noise in an interferometer,* Phys. Rev. D **23**, 1693-1708 (1981).

[22] Vittorio Giovannetti, Seth Lloyd, and Lorenzo Maccone, *Quantum-enhanced measurements: Beating the standard quantum limit,* Science **306**, 1330-1336 (2004).

[23] Vittorio Giovannetti, Seth Lloyd, and Lorenzo Maccone, *Quantum metrology,* Phys. Rev. Lett. **96**, 010401 (2006).

[24] Vittorio Giovannetti, Seth Lloyd, and Lorenzo Maccone, *Advances in quantum metrology,* Nat. Photon. **5**, 222-9 (2011).

[25] Sergio Boixo, Animesh Datta, Matthew J. Davis, Steven T. Flammia, Anil Shaji, and Carlton M. Caves, *Quantum metrology: Dynamics versus entanglement,* Phys. Rev. Lett. **101**, 040403 (2008).

[26] M. Napolitano and M. W. Mitchell, *Nonlinear metrology with a quantum interface,* New J. Phys. **12**, 093016 (2010).

[27] Alfredo Luis, *Nonlinear transformations and the heisenberg limit,* Phys. Lett. A **329**, 8 - 13 (2004).

[28] Alfredo Luis, *Quantum limits, nonseparable transformations, and nonlinear optics,* Phys. Rev. A **76**, 035801 (2007).

[29] A. M. Rey, L. Jiang, and M. D. Lukin, *Quantum-limited measurements of atomic scattering properties,* Phys. Rev. A **76**, 053617 (2007).

[30] S. M. Roy and Samuel L. Braunstein, *Exponentially enhanced quantum metrology,* Phys. Rev. Lett. **100**, 220501 (2008).

[31] S. Choi and B. Sundaram, *Bose-einstein condensate as a nonlinear ramsey interferometer operating beyond the heisenberg limit,* Phys. Rev. A **77**, 053613 (2008).

[32] M. J. Woolley, G. J. Milburn, and Carlton M. Caves, *Nonlinear quantum metrology using coupled nanomechanical resonators,* New J. Phys. **10**, 125018 (2008).

[33] Sergio Boixo, Animesh Datta, Matthew J. Davis, Anil Shaji, Alexandre B. Tacla, and Carlton M. Caves, *Quantum-limited metrology and Bose-Einstein condensates,* Phys. Rev. A **80**, 032103 (2009).

[34] Bradley A. Chase, Ben Q. Baragiola, Heather L. Partner, Brigette D. Black, and J. M. Geremia, *Magnetometry via a double-pass continuous quantum measurement of atomic spin,* Phys. Rev. A **79**, 062107 (2009).

[35] Alexandre B. Tacla, Sergio Boixo, Animesh Datta, Anil Shaji, and Carlton M. Caves, *Nonlinear interferometry with bose-einstein condensates,* Phys. Rev. A **82**, 053636 (2010).

[36] E. Tiesinga and P. R. Johnson, *Quadrature interferometry for nonequilibrium ultracold atoms in optical lattices,* Phys. Rev. A **87**, 013423 (2013).

[37] Juha Javanainen and Han Chen, *Optimal measurement precision of a nonlinear interferometer,* Phys. Rev. A **85**, 063605 (2012).

[38] Marcin Zwierz, Carlos A. Pérez-Delgado, and Pieter Kok, *General optimality of the heisenberg limit for quantum metrology,* Phys. Rev. Lett. **105**, 180402 (2010).

[39] Rafal Demkowicz-Dobrzanski, Jan Kolodynski, and Madalin Guta, *The elusive heisenberg limit in quantum-enhanced metrology,* Nat. Comm. **3**, 1063 (2012).

[40] Michael J. W. Hall and Howard M. Wiseman, *Does nonlinear metrology offer improved resolution? answers from quantum information theory,* Phys. Rev. X **2**, 041006 (2012).

[41] M. Koschorreck, M. Napolitano, B. Dubost, and M. W. Mitchell, *Quantum nondemolition measurement of large-spin ensembles by dynamical decoupling,* Phys. Rev. Lett. **105**, 093602 (2010).

[42] R. J. Sewell, M. Napolitano, N. Behbood, G. Colangelo, and M. W. Mitchell, *Certified quantum nondemolition measurement of a macroscopic material system,* Nat. Photon. **7**, 517-520 (2013).

[43] Caspar F. Ockeloen, Roman Schmied, Max F. Riedel, and Philipp Treutlein, *Quantum metrology with a scanning probe atom interferometer,* Phys. Rev. Lett. **111**, 143001 (2013).

[44] Dmitry Budker and Michael Romalis, *Optical magnetometry,* Nat. Phys. **3**, 227-234 (2007).

[45] G. Vasilakis, V. Shah, and M. V. Romalis, *Stroboscopic backaction evasion in a dense alkali-metal vapor,* Phys. Rev. Lett. **106**, 143601 (2011).

[46] N. Behbood, F. Martin Ciurana, G. Colangelo, M. Napolitano, M. W. Mitchell, and R. J. Sewell, *Real-time vector field tracking with a cold-atom magnetometer,* Appl. Phys. Lett. **102**, 173504 (2013).

[47] L. E. Sadler, J. M. Higbie, S. R. Leslie, M. Vengalattore, and D. M. Stamper-Kurn, *Spontaneous symmetry breaking in a quenched ferromagnetic spinor bose-einstein condensate,* Nature **443**, 312-315 (2006).

[48] M. Vengalattore, J. M. Higbie, S. R. Leslie, J. Guzman, L. E. Sadler, and D. M. Stamper-Kurn, *High-resolution magnetometry with a spinor bose-einstein condensate,* Phys. Rev. Lett. **98**, 200801 (2007).

[49] Y. Liu, E. Gomez, S. E. Maxwell, L. D. Turner, E. Tiesinga, and P. D. Lett, *Number fluctuations and energy dissipation in sodium spinor condensates,* Phys. Rev. Lett. **102**, 225301 (2009).

[50] Géza Tóth and Morgan W Mitchell, *Generation of macroscopic singlet states in atomic ensembles,* New J. Phys. **12**, 053007 (2010).

[51] P. Hauke, R. J. Sewell, M. W. Mitchell, and M. Lewenstein, *Quantum control of spin correlations in ultracold lattice gases,* Phys. Rev. A **87**, 021601 (2013).

[52] N. Behbood, G. Colangelo, F. Martin Ciurana, M. Napolitano, R. J. Sewell, and M. W. Mitchell, *Feedback cooling of an atomic spin ensemble,* Phys. Rev. Lett. **111**, 103601 (2013).

[53] G. Puentes, G. Colangelo, R. J. Sewell, and M. W. Mitchell, *Planar squeezing by quantum nondemolition measurement in cold atomic ensembles,* New J. Phys. **15**, 103031 (2013).

[54] K. Eckert, Ł. Zawitkowski, A. Sanpera, M. Lewenstein, and E. S. Polzik, *Quantum polarization spectroscopy of ultracold spinor gases,* Phys. Rev. Lett. **98**, 100404 (2007).

[55] Kai Eckert, Oriol Romero-Isart, Mirta Rodriguez, Maciej Lewenstein, Eugene S. Polzik, and Anna Sanpera, *Quantum nondemolition detection of strongly correlated systems,* Nat. Phys. **4**, 50-54 (2008).

[56] M. Kubasik, M. Koschorreck, M. Napolitano, S. R. de Echaniz, H. Crepaz, J. Eschner, E. S. Polzik, and M. W. Mitchell, *Polarization-based light-atom quantum interface with an all-optical trap,* Phys. Rev. A **79**, 043815 (2009).

[57] S. R. de Echaniz, M. W. Mitchell, M. Kubasik, M. Koschorreck, H. Crepaz, J. Eschner, and E. S. Polzik, *Conditions for spin squeezing in a cold 87 rb ensemble,* J. Opt. B **7**, S548 (2005).

[58] A. Kuzmich, N. P. Bigelow, and L. Mandel, *Atomic quantum nondemolition measurements and squeezing,* Europhys. Lett. **42**, 481 (1998).

[59] D. J. Wineland, J. J. Bollinger, W. M. Itano, F. L. Moore, and D. J. Heinzen, *Spin squeezing and reduced quantum noise in spectroscopy,* Phys. Rev. A **46**, R6797-R6800 (1992).

[60] G. Colangelo, R. J. Sewell, N. Behbood, F. Martin Ciurana, G. Triginer, and M. W Mitchell, *Quantum atom-light interfaces in the gaussian description for spin-1 systems,* New J. Phys. **15**, 103007 (2013).

[61] L. B. Madsen and K. Mølmer, *Spin squeezing and precision probing with light and samples of atoms in the gaussian description,* Phys. Rev. A **70**, 052324 (2004).

[62] Luca Pezzé and Augusto Smerzi, *Phase sensitivity of a mach-zehnder interferometer,* Phys. Rev. A **73**, 011801 (2006).